Tire Modeling to Enable Model Predictive Control of Automated Vehicles From Standstill to the Limits of Handling

Vivian Zhang, Sarah M. Thornton, & J. Christian Gerdes
Department of Mechanical Engineering
Stanford University, Stanford, California, USA

E-mail: zhangv@stanford.edu

Topics / Vehicle Automation and Connection, Vehicle Dynamics and Chassis Control

Model predictive control (MPC) frameworks have been effective in collision avoidance, stabilization, and path tracking for automated vehicles in real-time. These MPC formulations use a variety of vehicle models that capture specific aspects of vehicle handling, focusing either on low-speed scenarios or highly dynamic maneuvers. However, these models individually are unable to handle all operating regions with the same performance. This work introduces a novel linearization of a brush tire model that is affine, time-varying, and effective at any speed. We incorporate this tire model into a convex MPC formulation for lateral control on a low friction surface. Experimental results on an automated Volkswagen Golf GTI demonstrate effective steering control for path tracking from a standstill up to the limits of tire-road friction.

1 INTRODUCTION

Model predictive control (MPC) frameworks have been effective in collision avoidance, stabilization, and path tracking for automated vehicles [1], [2]. These control formulations utilize vehicle models to solve optimization problems in real-time and must therefore balance model accuracy and computational efficiency. As a result, vehicle models are tailored for high performance in a subset of the vehicle's operating regime, but at a cost of being less accurate or even unusable in others. The unique benefits and limitations of different vehicle models pose major hurdles when designing a cohesive controller that can handle both stop-and-go traffic and driving at the limits of tire-road friction.

The kinematic vehicle model is an attractive choice for path planning and tracking for normal driving scenarios with low lateral accelerations. It has acceptable online computational performance despite the nonlinearity of the model. Chu *et. al.* leverage the simplicity of the model to generate kinematically feasible trajectories for path planning and obstacle avoidance [3]. Schildbach and Borelli incorporate the kinematic model into an MPC approach for performing safe lane changes on highways [4]. But because the model assumes no tire slip and omits a model of tire-road interaction, it becomes unsuitable for control at high lateral accelerations. Incorporating a high-fidelity tire model would improve the prediction accuracy of the system dynamics across operating regimes. For example, the LuGre dynamic friction tire model accurately captures tire dynamics over a broad range of motion, even when crossing zero velocity [5], [6]. However, because this model utilizes a large number of states, the added computational load in integrating these states is prohibitive for robust real-time control. Especially for controllers that solve an optimization problem, such as model predictive control, this complexity limits the execution speed of the controller.

Dynamic vehicle models that incorporate a brush-tire model take into account tire slip, unlike the kinematic model, yet are much simpler and have fewer states than the LuGre model. These models have been integrated into various controllers for real vehicles up to the limits of friction when leveraging convex optimization techniques. Brown *et al.* developed a model predictive controller (MPC) that solves an optimization problem to handle the potentially competing objectives of vehicle stability and environmental constraints in real-time [1] . The optimization returns a series of lateral tire force inputs which is then converted into steer angle commands by inverting a brush tire model. Carvalho *et al*. used an iteratively linearized form of the dynamic vehicle model, and the vehicle was able to successfully maneuver around obstacles on low-friction, snowy roads [2]. However, both Brown and Carvalho estimate lateral tire forces generated by relying on tire slip angles, a parameter that becomes undefined at zero longitudinal speed. Existing ad-hoc solutions for stop-and-go maneuvers involve switching to a kinematic model or disabling the controller below a specific longitudinal speed. Although the dynamic vehicle model is effective for high speeds and lateral accelerations, the singularity at zero longitudinal speed prohibits the model from being effective in urban situations.

This paper presents a dynamic vehicle model that uses a modified tire model to predict accurate tire-road forces from standstill up to high lateral accelerations. The tire model leverages successive linearizations of the Fiala tire model to address the singularity at zero speed. No additional states or switching conditions are introduced, compromising neither run-time efficiency nor smooth behavior of the system. An overview of the dynamic vehicle model and the Fiala tire model is covered in section 2. Section 3 elaborates on the modifications for low-speed. This affine, time-varying model is validated in a convex MPC framework for lateral control, described in section 4, and experimental results from a full-scale autonomous vehicle are shown in section 5. In particular, the vehicle in Figure 1 is brought to a stop on a curved roadway as well as pushed to the limits on a snow-covered skidpad.

Figure 1: Automated Volkswagen Golf GTI vehicle research platform.

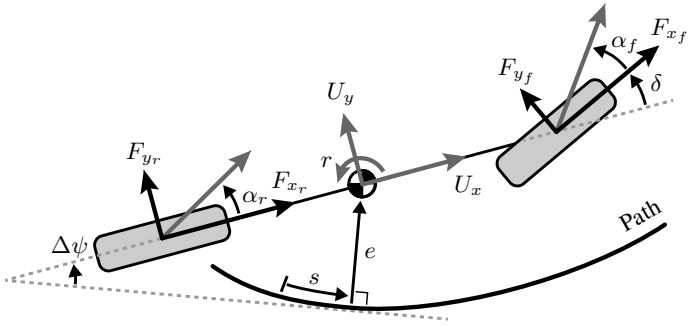

Figure 2: Single-track dynamic vehicle model along a path.

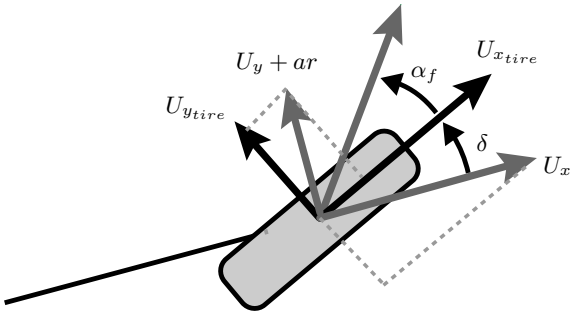

Figure 3: Front tire model with the longitudinal and lateral velocity at the axle. Front slip angle can be calculated by taking the velocity components along and perpendicular to the tire heading.

2 VEHICLE MODEL

The continuous-time dynamic bicycle model in Figure 2, with lumped front and rear wheels, has three vehicle states: longitudinal velocity U_x, lateral velocity U_y, and yaw rate r. Additionally, we consider three positional states relative to a desired path: the distance along the path s, the lateral error from the path e, and the angle from the road heading to the vehicle heading $\Delta\psi$. Assuming U_x, s, and path curvature κ are known and using small angle assumptions, the equations of motion that describe the lateral motion relative to a path are then

$$\dot{U}_\mathrm{y} = \frac{F_\mathrm{yf} + F_\mathrm{yr}}{m} - rU_\mathrm{x} \tag{1a}$$

$$\dot{r} = \frac{aF_\mathrm{yf} - bF_\mathrm{yr}}{I_\mathrm{z}} \tag{1b}$$

$$\dot{e} = U_\mathrm{x} + U_\mathrm{y}\Delta\psi \tag{1c}$$

$$\Delta\dot{\psi} = r - \kappa\dot{s} \tag{1d}$$

F_yf and F_yr are the lateral tire forces at the front and rear axles, respectively. m and I_z are the mass and yaw inertial of the vehicle, and a and b are distances from the center of mass to the front and rear axles, respectively.

The front lateral tire force is a nonlinear function of the front slip angle α_f, which is the angle from the tire heading to the velocity vector of the tire. This is defined in terms of the vehicle states and steer input δ as

$$\alpha_\mathrm{f} = \arctan\left(\frac{U_\mathrm{y} + ar}{U_\mathrm{x}}\right) - \delta \tag{2}$$

The front slip angle can also be written using a decomposition of the longitudinal and lateral velocities at the front axle, as in Figure 3. Taking the velocity components along and perpendicular to the tire heading,

$$\begin{bmatrix} U_{x_{tire}} \\ U_{y_{tire}} \end{bmatrix} = \begin{bmatrix} \cos\delta & \sin\delta \\ -\sin\delta & \cos\delta \end{bmatrix} \begin{bmatrix} U_\mathrm{x} \\ U_\mathrm{y} + ar \end{bmatrix}$$

$$= \begin{bmatrix} U_\mathrm{x}\cos\delta + (U_\mathrm{y} + ar)\sin\delta \\ -U_\mathrm{x}\sin\delta + (U_\mathrm{y} + ar)\cos\delta \end{bmatrix}$$

Front slip angle is therefore equivalently:

$$\alpha_\mathrm{f} = \arctan\frac{U_{y_{tire}}}{U_{x_{tire}}}$$

$$= \arctan\frac{-U_\mathrm{x}\sin\delta + (U_\mathrm{y} + ar)\cos\delta}{U_\mathrm{x}\cos\delta + (U_\mathrm{y} + ar)\sin\delta} \tag{3}$$

Notice that slip angle is defined assuming the vehicle is in motion and becomes undefined when the vehicle is at a standstill.

The single friction coefficient Fiala tire model as presented by Pacejka [7] describes the lateral tire forces generated using slip angle as an intermediate variable:

$$F_\mathrm{y} = \begin{cases} -C_\alpha \tan\alpha + \frac{C_\alpha^2}{3\mu F_\mathrm{z}}|\tan\alpha|\tan\alpha \\ \quad -\frac{C_\alpha^3}{27\mu^2 F_\mathrm{z}^2}\tan^3\alpha, & |\alpha| < \operatorname{atan}\left(\frac{3\mu F_\mathrm{z}}{C_\alpha}\right) \\ -\mu F_\mathrm{z}\operatorname{sgn}\alpha, & \text{otherwise} \end{cases} \tag{4}$$

where μ is the tire-road coefficient of friction, C_α is the tire cornering stiffness, and F_z is the normal load at the front or rear tire. The impact of longitudinal load transfer on the tire cornering behavior can be captured by modifying the normal loads in proportion to the longitudinal acceleration. The maximum lateral tire force available is also affected by the throttle and brake demands. A simplified coupled tire model is used to derate the maximum lateral tire force based on longitudinal forces at each tire. Using the friction circle as a constraint, the maximum lateral force can be calculated using

$$F_\mathrm{x}^2 + F_\mathrm{y,max}^2 = (\mu F_\mathrm{z})^2 \tag{5}$$

where F_x is the longitudinal control input.

For frameworks that require convexity, an affine approximation of the tire curve can be used. Erlien *et al.* approximate this nonlinear relation for the rear tires with an affine, time-varying model that uses successive linearization points [8]. A similar method can be applied at the front tires:

$$F_\mathrm{yf} = \left.\frac{\partial F_\mathrm{yf}}{\partial\alpha_\mathrm{f}}\right|_{\alpha_\mathrm{f,0}} (\alpha_\mathrm{f} - \alpha_\mathrm{f,0}) + F_\mathrm{yf}(\alpha_\mathrm{f,0}) \tag{6}$$

which is simply a Taylor expansion about an operating point $\alpha_\mathrm{f,0}$. Assuming small angles for equation (2) and using steer angle as the controller input, the system is represented by linear differential equations.

While these formulations are effective at nominal or high lateral forces, the calculation of slip angle assumes a non-zero longitudinal velocity and begins to break down at low speeds. Even if the denominator of the slip angle calculation was saturated at a minimum value, this model does not accurately capture low speed dynamics. If the vehicle is stopped, then regardless of the steer angle, no significant lateral forces are generated, and the vehicle is unable to move laterally.

3 LOW SPEED FORMULATION

The desired properties of an effective front tire model are (a) it is well-defined and continuous at any longitudinal velocity, (b) at zero longitudinal velocity, changing the steer angle has no effect on the lateral tire forces, and (c) at higher velocities and lateral accelerations, it approximates the Fiala tire model. Taking inspiration from the tire model in equation (4), we will formulate a modified tire model with these attributes.

An affine approximation to the front tire model can be formulated by using a first-order Taylor expansion with respect to the vehicle states and controller input directly. This bypasses calculating slip angles, which only exist at non-zero speed, as an intermediate step. The full Taylor expansion of the variables δ, U_y, and r about an operating point $p = (\delta_0, U_{y0}, r_0)$ is

$$\begin{aligned} F_{\text{yf}}(\delta, U_{\text{y}}, r) =& F_{\text{yf}}((\delta_0, U_{y0}, r_0)) + \left.\frac{\partial F_{\text{yf}}}{\partial \delta}\right|_p (\delta - \delta_0) + \\ & \left.\frac{\partial F_{\text{yf}}}{\partial U_{\text{y}}}\right|_p (U_{\text{y}} - U_{y0}) + \left.\frac{\partial F_{\text{yf}}}{\partial r}\right|_p (r - r_0) \end{aligned} \tag{7}$$

The partial derivative of the lateral tire force with respect to steer angle, lateral velocity, and yaw rate can be rewritten using the chain rule

$$\frac{\partial F_{\text{yf}}}{\partial \delta} = \frac{\partial F_{\text{yf}}}{\partial \tan \alpha_{\text{f}}} \frac{\partial \tan \alpha_{\text{f}}}{\partial \delta} \tag{8}$$

and similarly for the partial derivatives with respect to the states. Then using equations (3) and (4),

$$\frac{\partial F_{\text{yf}}}{\partial \tan \alpha_{\text{f}}} = -C_{\alpha_{\text{f}}} + \frac{2C_{\alpha_{\text{f}}}^2}{3\mu F_z} |\tan \alpha_{\text{f}}| - \frac{C_{\alpha_{\text{f}}}^3}{9\mu^2 F_z^2} \tan^2 \alpha_{\text{f}} \tag{9}$$

$$\frac{\partial \tan \alpha_{\text{f}}}{\partial \delta} = \frac{-(U_{\text{x}}^2 + (U_{\text{y}} + ar)^2)}{(U_{\text{x}} \cos \delta + (U_{\text{y}} + ar) \sin \delta)^2} \tag{10}$$

$$\frac{\partial \tan \alpha_{\text{f}}}{\partial U_{\text{y}}} = \frac{U_{\text{x}}}{(U_{\text{x}} \cos \delta + (U_{\text{y}} + ar) \sin \delta)^2} \tag{11}$$

$$\frac{\partial \tan \alpha_{\text{f}}}{\partial r} = \frac{aU_{\text{x}}}{(U_{\text{x}} \cos \delta + (U_{\text{y}} + ar) \sin \delta)^2} \tag{12}$$

The denominators of $\tan \alpha_{\text{f}}$ in equation (3) and (10)-(12) may still evaluate to zero when the vehicle is at rest. Utilizing these equations with added saturation allows us to define a modified tire model that has the desired properties listed at the beginning of this section.

We define the following variables ξ, ξ_{F_y}, and ξ_δ that are analogous to $\tan \alpha_{\text{f}}$ as expressed in equation (3), $\frac{\partial F_{\text{y}}}{\partial \tan \alpha}$ in equation (9), and $\frac{\partial \tan \alpha_{\text{f}}}{\partial \delta}$ in equation (10), respectively:

$$\xi \triangleq \frac{-U_{\text{x}} \sin \delta + (U_{\text{y}} + ar) \cos \delta}{\min(U_{\text{x}} \cos \delta + (U_{\text{y}} + ar) \sin \delta, \epsilon)} \tag{13}$$

$$\xi_{F_y} \triangleq -C_{\alpha_{\text{f}}} + \frac{2C_{\alpha_{\text{f}}}^2}{3\mu F_z} |\xi| - \frac{C_{\alpha_{\text{f}}}^3}{9\mu^2 F_z^2} \xi^2 \tag{14}$$

$$\xi_\delta \triangleq \frac{-(U_{\text{x}}^2 + (U_{\text{y}} + ar)^2)}{\min((U_{\text{x}} \cos \delta + (U_{\text{y}} + ar) \sin \delta)^2, \epsilon)} \tag{15}$$

The saturation value ϵ is chosen to be $0.5\,\text{m/s}$. The partial derivative of the lateral tire force with respect to steer angle using ξ is referred to as the *steering authority* of the system and can be redefined using the modified equation:

$$\frac{\partial F_{\text{yf}}}{\partial \delta} \triangleq \xi_{F_y} \xi_\delta \tag{16}$$

Using this formulation simultaneously produces a continuous, non-singular function at all longitudinal velocities and captures the desired behavior between longitudinal velocity and steering for lateral tire force generation. As U_{x} approaches $0\,\text{m/s}$, ξ_δ approaches 0. Figure 4 displays the relationship between longitudinal speed and ξ_δ using experimental data from a straight line deceleration. Since ξ_δ is directly related to $\frac{\partial F_{\text{yf}}}{\partial \delta}$, the steering authority also approaches $0\,\text{N/rad}$. When steering authority is zero, changing the steer angle has no impact on the forces generated at the front tires. This behavior is more accurate than the original linearization of the Fiala tire model at low speeds, where the lateral tire curve remains the same at all longitudinal speeds for well-defined slip angles. The modifications to the partial derivatives with respect to input only change the tire model behavior from the original Fiala model below $0.5\,\text{m/s}$. At higher longitudinal velocities, these models are exactly equal.

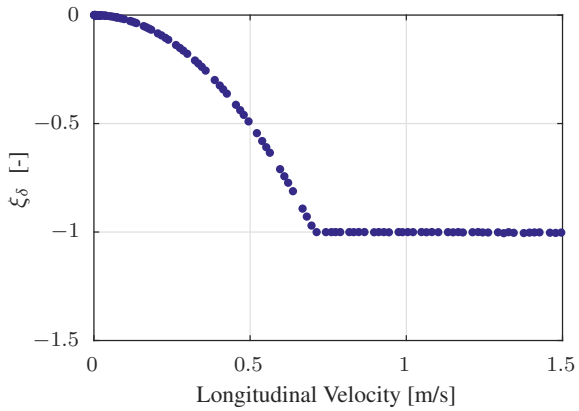

Figure 4: ξ_δ with a saturated denominator ϵ of $0.5\,\text{m/s}$. As the longitudinal velocity approaches a standstill, both ξ_δ and steering authority go to zero.

The partial derivatives with respect to lateral velocity and yaw rate, both for the front and the rear tires, can be modified in a similar manner. We define these partials for the front tires with our modified expressions as

$$\frac{\partial F_{\text{yf}}}{\partial U_{\text{y}}} \triangleq \xi_{F_y} \xi_{U_{\text{y}}} \tag{17}$$

$$\frac{\partial F_{\text{yf}}}{\partial r} \triangleq \xi_{F_y} \xi_r \tag{18}$$

where $\xi_{U_{\text{y}}}$ and ξ_r are equal to equations (11) and (12). For numerical stability, the minimum U_{x} used to calculate these expressions is set to $1 \times 10^{-6}\,\text{m/s}$. The resulting variables reflect the desired behavior: if the vehicle is sliding sideways or yawing with little or no longitudinal motion, then large lateral forces are being generated. The vehicle becomes an extremely stiff system as the longitudinal velocity approaches zero.

4 MODEL PREDICTIVE CONTROL FORMULATION

We incorporate this modified vehicle model into a convex model predictive control (MPC) framework for steering. MPC involves solving an optimization problem for a series of inputs over a finite, receding horizon. It can explicitly handle constraints on the system and find an optimal solution according to a cost function. Only the first input is commanded to the system, then the optimization problem is updated with current measurements and re-solved at the next time step.

The equations (1) are convex assuming the longitudinal information U_{x} and s are known throughout the prediction horizon and are not solved for in the same optimization as δ. To accomplish this, a desired speed profile is generated *a priori* and then tracked via a separate feedback-feedforward controller. Using the desired longitudinal behavior along the prediction horizon and accounting for weight transfer, the MPC formulation utilizes the coupled tire model to derate the available force for lateral motion.

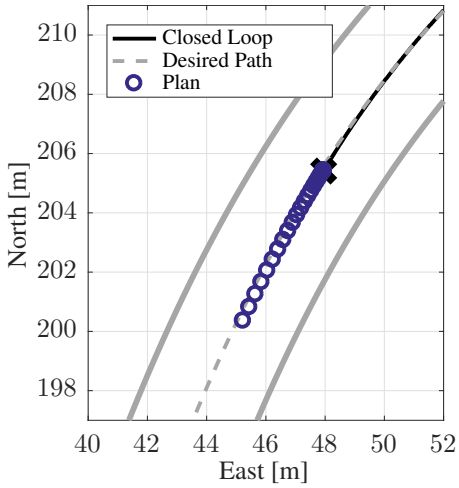

Figure 5: Snow-covered oval track. The vehicle is at a standstill in the turn but anticipates accelerating to resume tracking the desired speed and path over the prediction horizon.

These equations of motion in section 2 describe the continuous dynamic model, which is first linearized about an operating point, as described in section 3. The continuous-time matrices must subsequently be discretized at each step in the prediction horizon in order to be implemented in an MPC framework. The discretization of the these matrices via the matrix exponential not only provides an exact discretization, but it also consistently produces real-valued and bounded discrete time matrices for stiff systems. For the low-speed formulation in section 3, as the vehicle approaches zero longitudinal velocity, the magnitudes of the partial derivatives with respect to the states are large. Using the matrix exponential to discretize the system at each step in the prediction horizon numerically converts these large, negative, continuous-time derivatives into values approaching zero.

The metrics penalized in the cost function are the change in steer input between time steps, lateral error, and heading error from the path. Penalizing the rate of input change v in a weighting matrix R mitigates control effort and helps ensure smooth steering. A similar matrix Q for lateral and heading error promotes path tracking. Formally, the optimization problem for state vector $x = [U_y \quad r \quad \Delta\psi \quad e]^\top$ and input δ is

$$\underset{\delta}{\text{minimize}} \quad \sum_{k=0}^{n} v^{(k)\top} R^{(k)} v^{(k)} + \sum_{k=1}^{n} x^{(k)\top} Q^{(k)} x^{(k)} \tag{19a}$$

$$\text{subject to} \quad x^{(k+1)} = A^{(k)} x^{(k)} + B^{(k)} \delta^{(k)} + C^{(k)} \tag{19b}$$

$$|\delta^{(k)}| \leq \delta_{\max}^{(k)} \tag{19c}$$

$$|v^{(k)}| \leq v_{\max}^{(k)} \tag{19d}$$

where $v^{(k)} = \delta^{(k)} - \delta^{(k-1)}$ is the change in steer angle, and $\delta_{\max}^{(k)}$ and $v_{\max}^{(k)}$ are physical limits in the steering system. The matrices A, B, and C are constructed from equations (1) and (7) evaluated at $U_x^{(k)}$, $\kappa^{(k)}$, and operating points $\delta_0^{(k)}$, $U_{y0}^{(k)}$, and $r_0^{(k)}$.

5 EXPERIMENTAL RESULTS

We validate the model described in section 3 in a convex MPC formulation to control the automated Volkswagen Golf GTI depicted in Figure 1. The optimization problem runs at a rate of 100 Hz and is solved using CVXGEN, developed by Mattingley and Boyd [9]. The vehicle is equipped with a dual antenna Oxford Technical Solutions RT4003 integrated inertial navigation system and receives RTK differential correction information to measure position states within 2 cm accuracy.

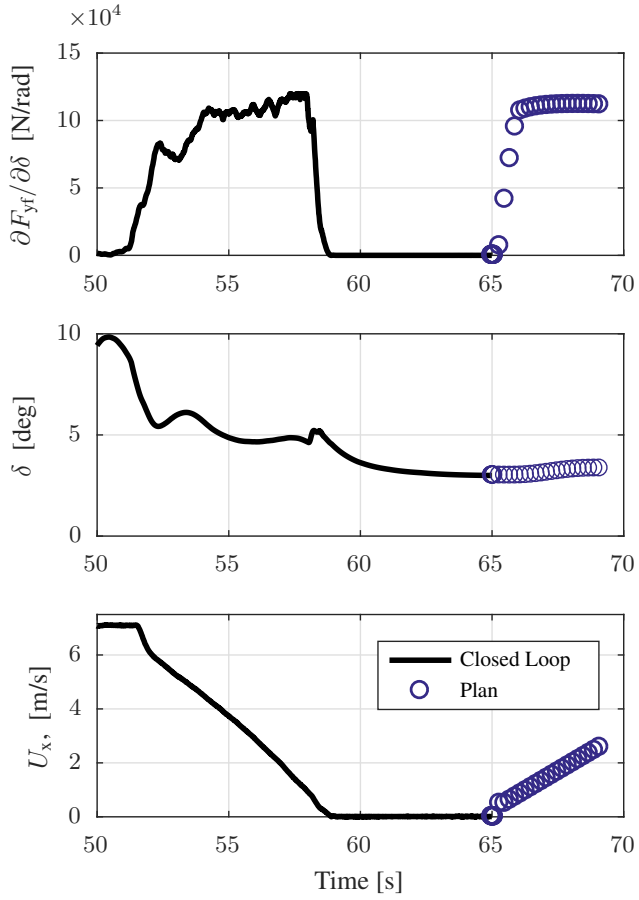

Figure 6: Closed-loop and planned steering authority (top), steer angle (middle), and longitudinal speed (bottom) plots for a stopping maneuver on a curved path. When at a standstill, the vehicle has zero steering authority to change the lateral tire forces produced.

We evaluate the path-tracking performance of the controller with a stop-and-go maneuver as well as a high lateral acceleration corner on a low friction track near the Arctic circle. The *a priori* estimates of the road friction μ range from 0.26 to 0.32. The MPC formulation optimistically uses a friction coefficient 0.32 in the tire-road model.

5.1 Stop-and-Go

The vehicle navigates the track at a constant 7.1 m/s according to a speed profile until the corner exit of the oval, where the speed profile goes to zero speed at a comfortable braking acceleration of $-2\,\text{m/s}^2$.

The lateral controller steers smoothly around the curved section of the track shown in Figure 5 even as the longitudinal controller brings the vehicle to a complete stop. In the closed-loop trajectory in Figure 6, as the longitudinal speed approaches zero, the steering authority also quickly decreases to zero. When the vehicle is stopped, no additional forces will be generated by steering according to this model. The solution to the optimization problem holds the steer angle at $\delta = 3.1°$. Because the system lacks steering authority when stopped, this steer angle approaches the Ackermann steer angle that is needed to track the path kinematically. For a vehicle with length $L = 2.63$ m following a path with local curvature $\kappa = 0.0237/\text{m}$,

$$\delta_{\text{acker}} = \text{atan}\left(\frac{L}{R}\right) = 3.46°.$$

The steady-state steer angle is therefore appropriate for tracking the path from a standstill. The controller plans to resume its original trajectory when an external signal indicates that it is safe to proceed. As seen in the horizon in Figure 6, this model predicts that as the longitudinal velocity increases, the steering authority is regained.

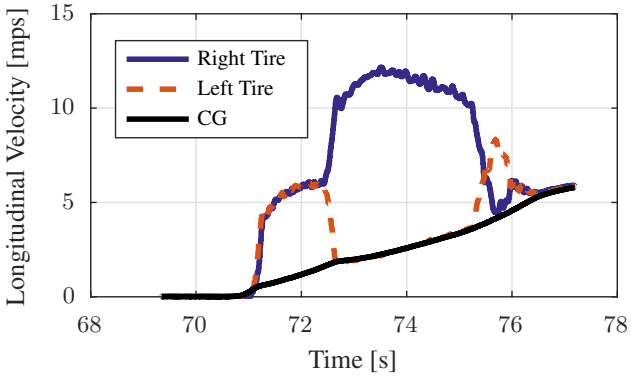

Figure 7: Longitudinal velocity measured at the center of gravity of the vehicle and estimated using wheel speed sensors of each the front tires.

When the stop indicator is removed, the desired speed returns to the original 7.1 m/s. Figure 7 shows the longitudinal speed at the center of gravity as compared to the longitudinal speed at both front tires, estimated from wheel speed sensors. The vehicle applies a large amount of longitudinal force at t = 71.1s to accelerate on the slippery surface and initially does not gain traction on either of the front wheels. As seen in Figure 8, the vehicle yaws to the right unexpectedly, and lateral tire forces are generated. In conjunction with the relatively aggressive longitudinal acceleration and the fact that the vehicle is front-wheel drive, the front tires approach friction limits at t = 71.8s. The longitudinal throttle demands derate the maximum lateral tire force available, and steering authority decreases abruptly. A similar phenomenon occurs at t = 72.8s.

Additionally, the vehicle stopped with a lateral error of 0.08 m and a heading error of $-0.75°$. Because the front tires spin and the vehicle slips forward longitudinally, the vehicle overshoots the path, unable to generate significant lateral tire forces to turn to the left until the left tire gains traction at t = 72.4s. Despite this, the maximum lateral error is just over 16 cm during this maneuver.

Because the vehicle has an open differential, while the front left wheel gains traction, the right front wheel continues to spin due to a locally polished surface of the track. The front left wheel is able to maneuver the vehicle to return to the path. When the vehicle regains traction on both tires at t = 75.25s, the controller resumes tracking the path normally. The vehicle recovers from the disturbance, and the planned trajectory resumes matching the closed-loop response. With the modified tire model, the steering controller handles even this extreme case of high wheel slip at very low vehicle speed.

5.2 Limit Path Tracking

The vehicle also performs well in terms of path-tracking and stability when experiencing high lateral accelerations, despite an overestimate in the available tire-road friction coefficient used in the model. Assuming the surface friction is $\mu = 0.32$, the maximum steady-state longitudinal velocity that is achievable before sliding is 6.7 m/s. Circumnavigating the oval at the slightly higher speed of 7.1 m/s, the vehicle fully saturates the vehicle's front and rear tires in the corner depicted in Figure 9 but manages to stay within 35 cm of the desired path. The prediction horizons in Figure 10 are shown at time t = 18.49s. The plan predicts that steering authority decreases as the vehicle reaches the apex of the turn. In closed-loop, because the available surface friction is lower than the actual value, the front tires fully saturate between t = 21.2s and t = 22.2s. When the tires are saturated, the model accurately determines that there is no steering authority, and changing the steer angle will not produce additional lateral tire force. The vehicle understeers since it is attempting a maneuver beyond the friction limits, but the steer angle does not grow unnecessarily large in the process.

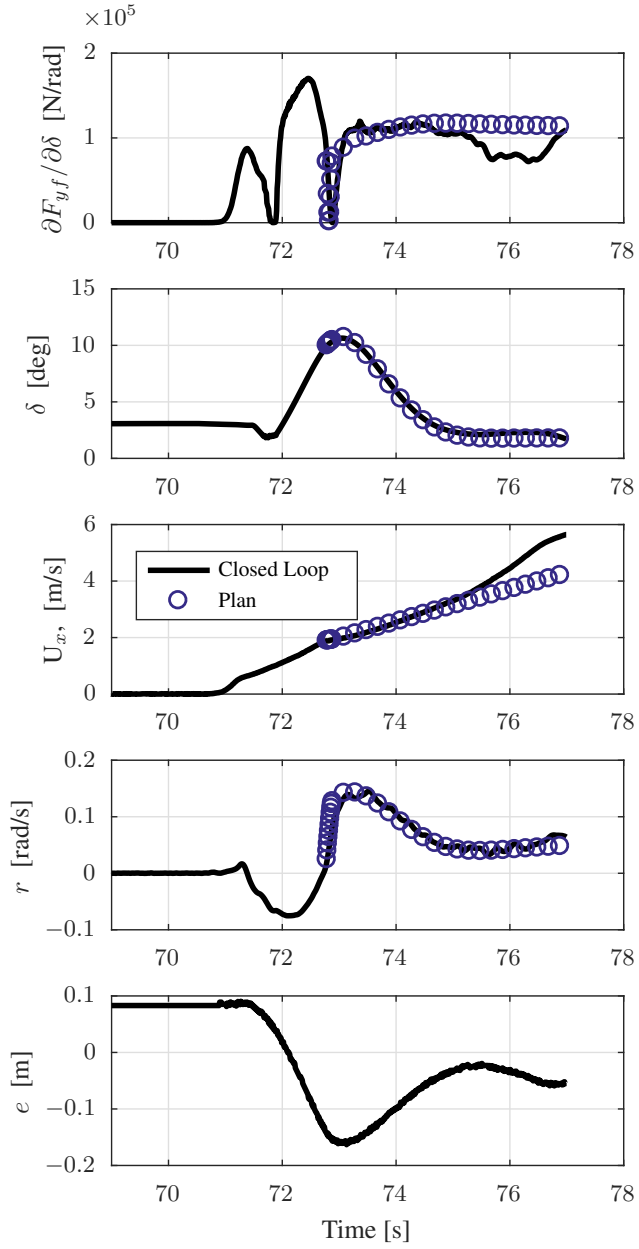

Figure 8: Accelerating from a standstill. As the vehicle yaws unexpectedly starting at t = 71.2s (bottom), in conjunction with the relatively aggressive longitudinal acceleration, the steering authority (top) drops. Once traction is gained on the left tire at t = 72.8s, the controller recovers from the disturbance and continues as planned.

6 CONCLUSIONS

We develop a dynamic vehicle model that can track a desired path from a complete standstill to cornering at the limits of handling by incorporating an affine tire model linearized with respect to the states and input directly. The tire model demonstrates the desired properties of being well-defined at all longitudinal velocities, having no steering authority at zero speed, and being exactly equal to the Fiala tire model at high longitudinal velocities. This formulation is validated in a model predictive control scheme experimentally on a low friction oval track. The MPC controller continues steering in an appropriate manner to track the curve even as the longitudinal controller brings the vehicle to a stop and slip angle becomes undefined. When the vehicle accelerates back to the desired speed, the model accurately responds to the yaw rate disturbance and the longitudinal forces derating the total amount of available lateral tire force. Because of a lack of available tire force, the controller predicts that steering authority is zero and the vehicle avoids overcorrecting for understeer.

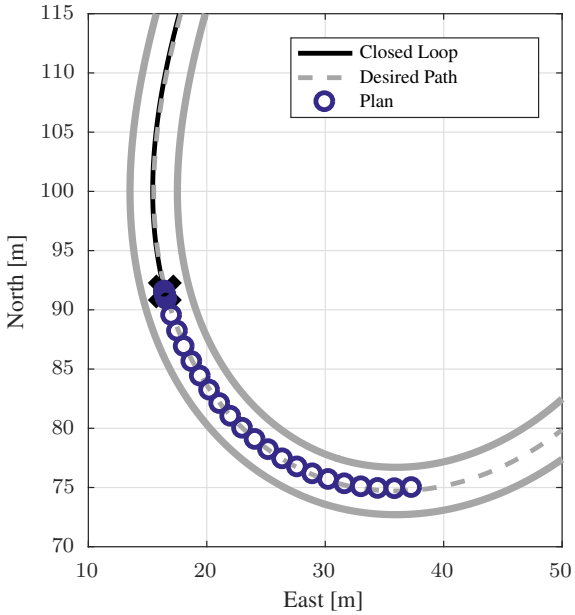

Figure 9: Prediction horizon during a high lateral acceleration corner.

7 ACKNOWLEDGEMENTS

Sarah Thornton and Vivian Zhang are supported by the Ford Motor Company through the Ford-Stanford Alliance. The authors would like to thank Volkswagen Group Research for providing the test vehicle, generously sharing the testing facilities, and facilitating collaboration and discussion. Many thanks to the Dynamic Design Lab, as always, for the thoughtful support and patience throughout.

REFERENCES

[1] M. Brown, J. Funke, S. Erlien, and J. C. Gerdes, "Safe Driving Envelopes for Path Tracking in Autonomous Vehicles," *Control Engineering Practice*, 2015.

[2] A. Carvalho, Y. Gao, A. Gray, H. E. Tseng, and F. Borrelli, "Predictive control of an autonomous ground vehicle using an iterative linearization approach," *IEEE Conference on Intelligent Transportation Systems, Proceedings, ITSC*, no. Itsc, pp. 2335–2340, 2013.

[3] K. Chu, S. Member, M. Lee, S. Member, and M. Sunwoo, "Local Path Planning for Off-Road Autonomous Driving With Avoidance of Static Obstacles," vol. 13, no. 4, pp. 1599–1616, 2012.

[4] G. Schildbach and F. Borrelli, "Scenario Model Predictive Control for Lane Change Assistance on Highways," in *IEEE Intelligent Vehicles Symposium*, 2015.

[5] C. Canudas de Wit, H. Olsson, K. Astrom, and P. Lischinsky, "A new model for control of systems with friction," *IEEE Transactions on Automatic Control*, vol. 40, no. 3, pp. 419–425, 1995.

[6] E. Velenis, P. Tsiotras, and C. Canudas-de Wit, "Extension of the lugre dynamic tire friction model to 2d motion," *Proceedings of the 10th IEEE Mediterranean Conference on Control and Automation-MED2002*, no. January 2002, pp. 9–12, 2002.

[7] H. Pacejka, *Tire and Vehicle Dynamics*, 3rd. Butterworth-Heinemann, 2012, p. 672. arXiv: `arXiv:1011.1669v3`.

[8] S. M. Erlien, J. Funke, and J. C. Gerdes, "Incorporating non-linear tire dynamics into a convex approach to shared steering control," *Proceedings of the American Control Conference*, pp. 3468–3473, 2014.

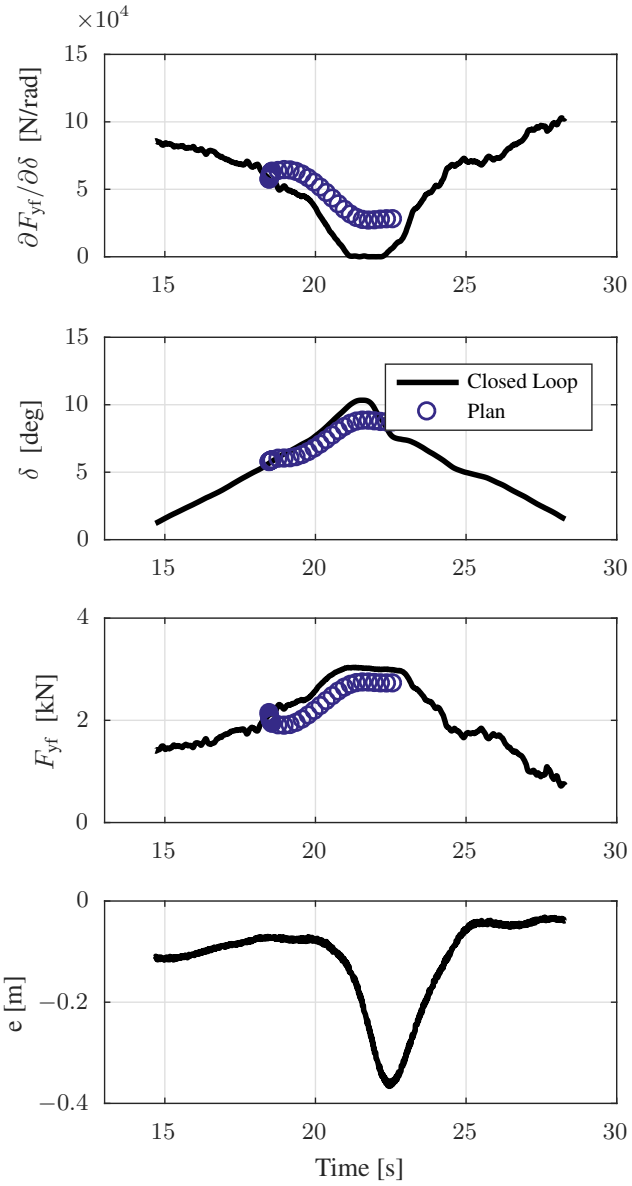

Figure 10: High lateral acceleration turn with fully saturated front tires. The prediction horizon in steering authority (top) is saturated at the apex of the curve. The maximum lateral error (bottom) is within 35 cm of the path.

[9] J. Mattingley and S. Boyd, "CVXGEN : a code generator for embedded convex optimization," *Optimization and Engineering*, vol. 13, no. 1, pp. 1–27, 2012.